GEOPHYSICS, VOL. 66, NO. 3 (MAY-JUNE 2001); P. 890–896, 4 FIGS., 2 TABLES.

Short Note

Numerical simulation of the Biot slow wave in water-saturated Nivelsteiner Sandstone

Børge Arntsen* and José M. Carcione‡

INTRODUCTION

The development of rock acoustic models is important for interpreting seismic data. These models should relate seismic properties such as wave velocity and attenuation to the production and lithological properties of reservoir rocks, such as porosity, permeability, fluid type, and fluid saturation.

As is well known (Biot, 1962), two *P*-waves propagate in a saturated porous medium. Plona (1980) was the first to observe the second (slow) *P*-wave in water-saturated sintered glass beads. Following this observation, Nagy et al. (1990) and Boyle and Chotiros (1992) detected the slow wave in thin slabs of air-filled sandstone and in water-saturated unconsolidated sand, respectively. Comparisons between theory and experiment were performed by Teng (1990), who used a finite-element algorithm, and Gurevich et al. (1999), who used the OASES modeling code (Schmidt and Tango, 1986), based on a reflectivity algorithm. Gurevich et al. (1999) performed experiments on a sample made of sintered glass beads and used the Biot's pore-form factor as a fitting parameter. This factor controls the behavior of the dynamic permeability/tortuosity function. However, although this approach successfully describes the wave propagation properties of synthetic porous media such as sintered glass beads, in natural porous media, such as sandstone, discrepancies between Biot's theory and measurements are the result of complex pore shapes and the presence of clay, which are not present in synthetic media. This complexity gives rise to a variety of relaxation mechanisms that contribute to the attenuation of the different wave modes. Stoll and Bryan (1970) show that attenuation is controlled by the anelasticity of the skeleton (friction at grain contacts) and by viscodynamic causes. Chin et al. (1985) have analyzed Plona's data and are able to assess the attenuation in Plona's experiments. They use a generalized ray expansion algorithm, where multiple reflections and converted modes can be identified easily.

Kelder and Smeulders (1997) present experimental data of slow-wave propagation in a natural water-saturated sandstone, which can be representative of overpressured hydrocarbon reservoir sandstones. These acoustic experiments in the laboratory can be used to verify and calibrate a suitable theory for computing synthetic seismograms. The experiment conducted by Kelder and Smeulders (1997) provides such a basis for theory and numeric algorithm verification. They obtain transmission microseismograms through a plate made of a clean, unconsolidated natural sandstone, where all the events predicted by Biot's theory can be observed. The experiment provides, under controlled conditions, the traveltimes and relative amplitudes of the fast and slow compressional waves and the shear wave. A first attempt to model Kelder and Smeulders' microseismograms is performed by Bordakov et al. (1999), using a semianalytical approach based on plane-wave theory and inverse Fourier transformation. They show that Biot's theory properly predicts the traveltimes but yields much higher amplitudes for the multiple reflections, the slow wave, and the shear wave. Then, they use the BISQ model (Dvorkin et al., 1994) to incorporate the squirt-flow mechanism in Biot's theory. The slow wave disappears, in contrast with the experiments, and the modified theory cannot predict the relative amplitude between the fast waves.

In this work we attempt to model the microseismograms by using Biot's theory, introducing stiffness and viscodynamic dissipation based on viscoelastic theory to model additional attenuation mechanisms. This approach was proposed by Carcione (1998) to model relaxation mechanisms arising from the interaction between the skeleton and the pore fluid. In Carcione (1998), the Biot solid-grain/pore-fluid coupling modulus is generalized to a time-dependent relaxation function. We show that the experimental attenuation levels observed by Kelder and Smeulders (1997) can be modeled by making viscoelastic (complex and frequency dependent) the rigidity modulus

Manuscript received by the Editor September 14, 1999; revised manuscript received August 11, 2000.
*Statoil Research Center, Postuttak, N-7004, Trondheim, Norway. E-mail: barn@statoil.no.
‡Istituto Nazionale di Oceanografia e di Geofisica Sperimentale (OGS), Borgo Grotta Gigante 42c, 34010 Sgonico, Trieste, Italy. E-mail: jcarcione@ogs.trieste.it.

and the fluid viscosity/permeability factor, in addition to the above-mentioned coupling modulus. The modeling algorithm is parameterized with the dry-rock bulk and rigidity moduli and the tortuosity to match the observed traveltimes, with the quality factors associated to the relaxation functions to match the observed amplitudes. However, unlike Biot's theory, the algorith's present viscoelastic extension is based on a phenomenological model that cannot be used as a predictive tool.

To our knowledge, this is the first attempt to model an ultrasonic laboratory experiment (including slow-wave data) using a numeric algorithm based on a grid differential method for solving the poroelastic equations. The calibrated seismic modeling code can be used to compute synthetic seismograms under general conditions of material variability.

POROELASTIC THEORY

The constitutive equations for an isotropic poroelastic medium under plane strain conditions are given by (Biot, 1962)

$$\tau_{xx,t} = E v_{x,x} + (E - 2\mu) v_{z,z} + \alpha M \epsilon + s_x, \quad (1)$$

$$\tau_{zz,t} = (E - 2\mu) v_{x,x} + E v_{z,z} + \alpha M \epsilon + s_z, \quad (2)$$

$$\tau_{xz,t} = \mu (v_{x,z} + v_{z,x}) + s_{xz}, \quad (3)$$

$$p_{,t} = -M\epsilon + s_f, \quad (4)$$

and

$$\epsilon = \alpha (v_{x,x} + v_{z,z}) + q_{x,x} + q_{z,z}, \quad (5)$$

where τ_{xx}, τ_{zz}, and τ_{xz} are the total stress components, p is the fluid pressure, v and q are the solid and fluid (relative to the solid) particle velocities, and s_x, s_z, s_{xz}, and s_f are the external sources of stress for the solid and the fluid, respectively. The subscript x denotes $\partial/\partial x$.

The elastic coefficients are given by

$$E = K_m + \frac{4}{3}\mu, \quad (6)$$

$$M = \frac{K_s^2}{D - K_m}, \quad (7)$$

$$D = K_s\left[1 + \phi\left(K_s K_f^{-1} - 1\right)\right], \quad (8)$$

and

$$\alpha = 1 - \frac{K_m}{K_s}, \quad (9)$$

with K_m, K_s, and K_f the bulk moduli of the drained matrix, solid, and fluid, respectively; ϕ the porosity; and μ the shear modulus of the drained (and saturated) matrix. The stiffness E is the P-wave modulus of the dry skeleton, M is the coupling modulus between the solid and the fluid, and α is the poroelastic coefficient of effective stress.

One of the poroelastic equations of motion is Biot-Newton's dynamic equations (Biot, 1962):

$$\tau_{xx,x} + \tau_{xz,z} = \rho v_{x,t} + \rho_f q_{x,t} \quad (10)$$

and

$$\tau_{xz,x} + \tau_{zz,z} = \rho v_{z,t} + \rho_f q_{z,t}, \quad (11)$$

where

$$\rho = (1 - \phi)\rho_s + \phi \rho_f$$

is the composite density, with ρ_s and ρ_f the solid and fluid densities, respectively. Another poroelastic equation of motion is the dynamic Darcy's law:

$$-p_{,x} = \rho_f v_{x,t} + m q_{x,t} + b * q_{x,t} \quad (12)$$

and

$$-p_{,z} = \rho_f v_{z,t} + m q_{z,t} + b * q_{z,t}, \quad (13)$$

where $m = T\rho_f/\phi$, with T the tortuosity, b a relaxation function (see next section), and $*$ as time convolution. At low frequencies $b = H(t)\eta/\kappa$, where H is the Heaviside function, η is the fluid viscosity, and κ is the permeability of the medium.

The phase velocities and attenuation factors as a function of frequency can be found, for instance, in Carcione (1998) [equations (26) and (27), respectively]. Let us denote these quantities by c and $\alpha_{(\bullet)}$ and the fast compressional, slow compressional, and shear waves with the labels P_+, P_-, and S, respectively.

EXTENSION TO THE POROVISCOELASTIC CASE

Viscoelasticity is introduced into Biot's poroelastic equations for modeling attenuation related to the potential energy (stiffness dissipation) and the kinetic energy (viscodynamic dissipation) (Biot, 1962; Dvorkin et al., 1994; Carcione, 1996). Stiffness dissipation is described in the stress–strain relation, and viscodynamic dissipation is a dynamic permeability effect attributable to frequency-dependent interaction between the pore fluid and the solid matrix (e.g., Johnston et al., 1987). In the first case, the stiffnesses E, μ, and M are generalized to time-dependent relaxation functions, which we denote, in general, by $\psi(t)$. We assume that $\psi(0) = \psi_0$ equals the respective Biot modulus, i.e., we obtain Biot's poroelastic constitutive equations at high frequencies. Assume that the relaxation functions are described by a single Zener model,

$$\psi(t) = \psi_0 \frac{\tau_\sigma}{\tau_\epsilon}\left[1 + \left(\frac{\tau_\epsilon}{\tau_\sigma} - 1\right)\exp(-t/\tau_\sigma)\right]H(t), \quad (14)$$

where τ_ϵ and τ_σ are relaxation times. In the absence of experimental values for attenuation versus frequency, we consider the simplest model, that is, a single relaxation peak for each modulus with peak frequency close to the frequency of the transducers.

Viscoelasticity implies that multiplications of bulk moduli by field variables in equations (1)–(5) be replaced by time convolutions. For instance, in equation (1) these products are $E(v_{x,x}+v_{z,z})$, $\mu v_{z,z}$, and $\alpha\epsilon$. We substitute them by $\psi * u_{,t}$, where ψ denotes the relaxation function corresponding to E, μ, or M and u denotes $v_{x,x} + v_{z,z}$, $\mu v_{z,z}$, or $\alpha\epsilon$. As in the single-phase viscoelastic case (Carcione, 1995), we introduce memory variables to avoid the time convolutions. Then, the terms $\psi * u_{,t}$ are substituted by $\psi_0 u + e$, where e is the memory variable. Five memory variables are related to the constitutive equations, which satisfy the differential equation

$$e_{,t} = \psi_0\left(\frac{1}{\tau_\epsilon} - \frac{1}{\tau_\sigma}\right)u - \frac{e}{\tau_\sigma}. \quad (15)$$

Those variables are $e=(\psi'_{,t}H)*u$, where ψ' multiplies the Heaviside function in equation (14), that is, $\psi=\psi' H$.

On the other hand, viscodynamic dissipation introduces two additional memory variables because of the time-dependent relaxation function $b(t)$. Hence,

$$b(t)=\frac{\eta}{\kappa}\left[1+\left(\frac{\tau_\epsilon}{\tau_\sigma}-1\right)\exp(-t/\tau_\sigma)\right]H(t). \qquad (16)$$

The terms $b*u_{,t}$ are substituted by $b(0)u+e$, and the memory-variable equations have the form

$$e_{,t}=-\frac{1}{\tau_\sigma}\left[\frac{\eta}{\kappa}\left(\frac{\tau_\epsilon}{\tau_\sigma}-1\right)u+e\right], \qquad (17)$$

where the memory variables are $(b'_{,t}H)*q_x$ and $(b'_{,t}H)*q_z$, with b' defined by the expression $b=b'H$.

In the frequency domain, the time convolution $\psi*u$ is replaced by $\bar{\psi}\bar{u}$, where the bar indicates time Fourier transform. We obtain from equation (14)

$$\bar{\psi}=\psi_0\frac{\tau_\sigma}{\tau_\epsilon}\left(\frac{1+i\omega\tau_\epsilon}{1+i\omega\tau_\sigma}\right), \qquad (18)$$

and each complex modulus is denoted by $\bar{E}$, $\bar{\mu}$, and $\bar{M}$.

The relaxation times can be expressed in terms of a Q factor Q_0 and a reference frequency f_0 as

$$\tau_{\epsilon(\sigma)}=\frac{1}{2\pi f_0 Q_0}\left[\sqrt{Q_0^2+1}\pm 1\right], \qquad (19)$$

where τ_ϵ corresponds to the plus sign and τ_σ corresponds to the minus sign.

On the other hand, the frequency-domain viscodynamic operator has the form

$$\bar{b}=\frac{\eta}{\kappa}\left(\frac{1+i\omega\tau_\epsilon}{1+i\omega\tau_\sigma}\right). \qquad (20)$$

The functional dependence of $\bar{b}$ on ω is not that predicted by models of dynamic fluid flow. A physical dynamic permeability function is given, for instance, in Johnson et al. (1987). Here, we intend to model the viscodynamic operator in a narrow band about the frequency used in the laboratory experiment. The advantage of using equation (20) is the easy implementation in time-domain numerical modeling.

The phase velocities and attenuation factors are obtained from equations (26) and (27) of Carcione (1998) by substituting E, μ, M, and η/κ by $\bar{E}$, $\bar{\mu}$, $\bar{M}$, and $\bar{b}$, respectively.

MODELING THE ACOUSTIC PROPERTIES

The Nivelsteiner Sandstone sample used by Kelder and Smeulders (1997) in their experiment is a Miocene quartz sand with very low clay content. It has an average grain distribution of 100 to 300 μm. The material properties of Nivelsteiner Sandstone are given in Table 1. For simplicity we assume that the grains are made of pure quartz. We obtain the matrix properties by fitting the experimental data provided by Kelder and Smeulders (1997) at 500 kHz and by assuming that the level of dissipation is predicted by Biot's theory. First, we compute the shear modulus of the dry rock, μ, by fitting the shear-wave velocity of the saturated rock. Second, the dry-rock bulk modulus, K_m, is obtained by fitting the compressional velocity of the saturated rock. Finally, the tortuosity, T, is used as a free parameter to fit the experimental slow-wave velocity. The properties of the saturated rock at 500 kHz are given in Table 2. They are within the experimental errors given by Kelder and Smeulders (1997). In addition, the properties for the poroviscoelastic case are indicated. The introduction of viscoelastic effects is necessary to model the relative amplitudes between the different events. Figure 1 shows the phase velocities of the (a) fast, (b) slow, and (c) shear wave as a function of frequency. The squares and error bars correspond to the experimental data of Kelder and Smeulders (1997). Biot's velocities are represented by the broken lines, and the solid lines correspond to the poroviscoelastic case (see below). The slow wave is a propagation mode at 500 kHz.

To model the correct level of relative attenuation between the different events, we generalize μ, M, and b to relaxation functions, with $Q_0^\mu=10$, $Q_0^M=10$, and $Q_0^b=2$, respectively, and a relaxation-peak frequency of 250 kHz. Figure 2 shows the attenuation factors versus frequency, compared to those of Biot's poroelastic theory (Carcione, 1998). The viscodynamic relaxation function $b(t)$ affects mainly the attenuation of the slow wave. The attenuation values in the absence of viscodynamic loss are 0.48, 1.98, and 2.2 dB for the fast P-, slow P-, and shear waves, respectively.

SIMULATIONS

The experimental setup is shown in Figure 3 (top). A sample of Nivelsteiner Sandstone 21 mm thick, immersed in water, is mounted on a rotating table. The traces are obtained for several values of angle θ. The experimental results are shown in Figure 4 (top), where the traces are plotted versus the angle of incidence θ. The events were identified as the fast compressional wave (*FP*), the shear wave (*S*), the first multiple reflection of the fast compressional wave (*FFP*), and the slow wave (*SP*). A 2-D cross-section of this model is discretized on a mesh with 238×238 gridpoints and a grid

Table 1. Material properties.

Material	Property	Value
Grain	Bulk modulus, K_s	36.0 GPa
	Density, ρ_s	2650 kg/m^3
Matrix	Bulk modulus, K_m	6.21 GPa
	Shear modulus, μ	4.55 GPa
	Porosity, ϕ	0.33
	Permeability, κ	5 Darcies
	Tortuosity, T	2.14
Water	Bulk modulus, K_w	2.223 GPa
	Density, ρ_w	1000 kg/m^3
	Viscosity, η_w	1 cP

Table 2. Properties of the saturated rock at 500 kHz.

Value	Biot's theory	Viscoelastic theory	Experiment
c_{P+}	2814 m/s	2801 m/s	2810 ± 40 m/s
α_{P+}	3.4×10^{-3} dB	0.48 dB	—
c_{P-}	869 m/s	860 m/s	870 ± 20 m/s
α_{P-}	0.29 dB	2.27 dB	—
c_S	1527 m/s	1498 m/s	1515 ± 25 m/s
α_S	2.1×10^{-2} dB	2.22 dB	—
ρ	2105 kg/m^3	2105 kg/m^3	—

spacing $D_X = D_Z = 0.5$ mm. Figure 3 (bottom) shows the model and the source–receiver configuration. Rectangular strips of 40 gridpoints in length are used to absorb unphysical events coming from the boundaries of the mesh (this region is not shown in the figure). In the simulations we rotate the transmitter and the receiver instead of the rock sample. Water is modeled by setting $K_m = \mu_m = 0$, $K_s = K_w$, and $\rho_s = \rho_w$. The source is applied at the frame and the fluid (bulk source), such that

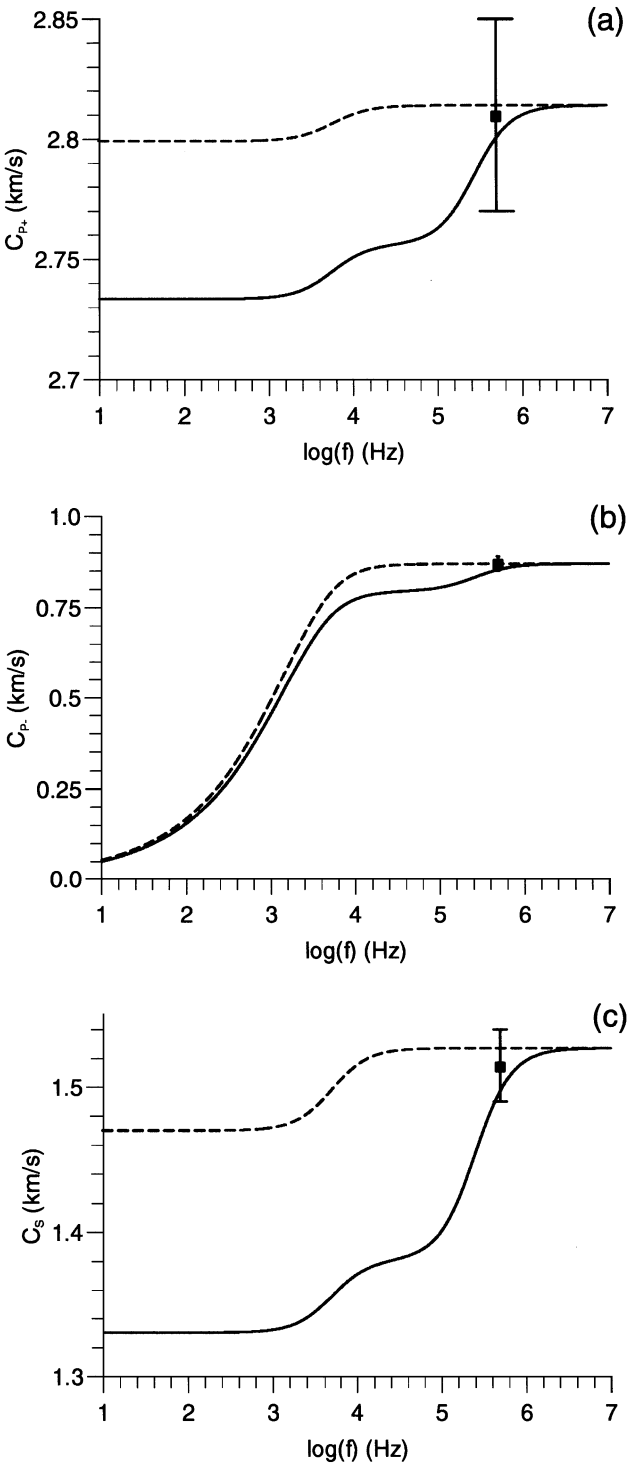

FIG. 1. Phase velocity of the (a) fast, (b) slow, and (c) shear waves as a function of frequency. The solid lines correspond to the poroviscoelastic case; the broken lines correspond to Biot's poroelastic theory. The experimental velocities, with corresponding error bars, given by Kelder and Smeulders (1997) are represented by black squares.

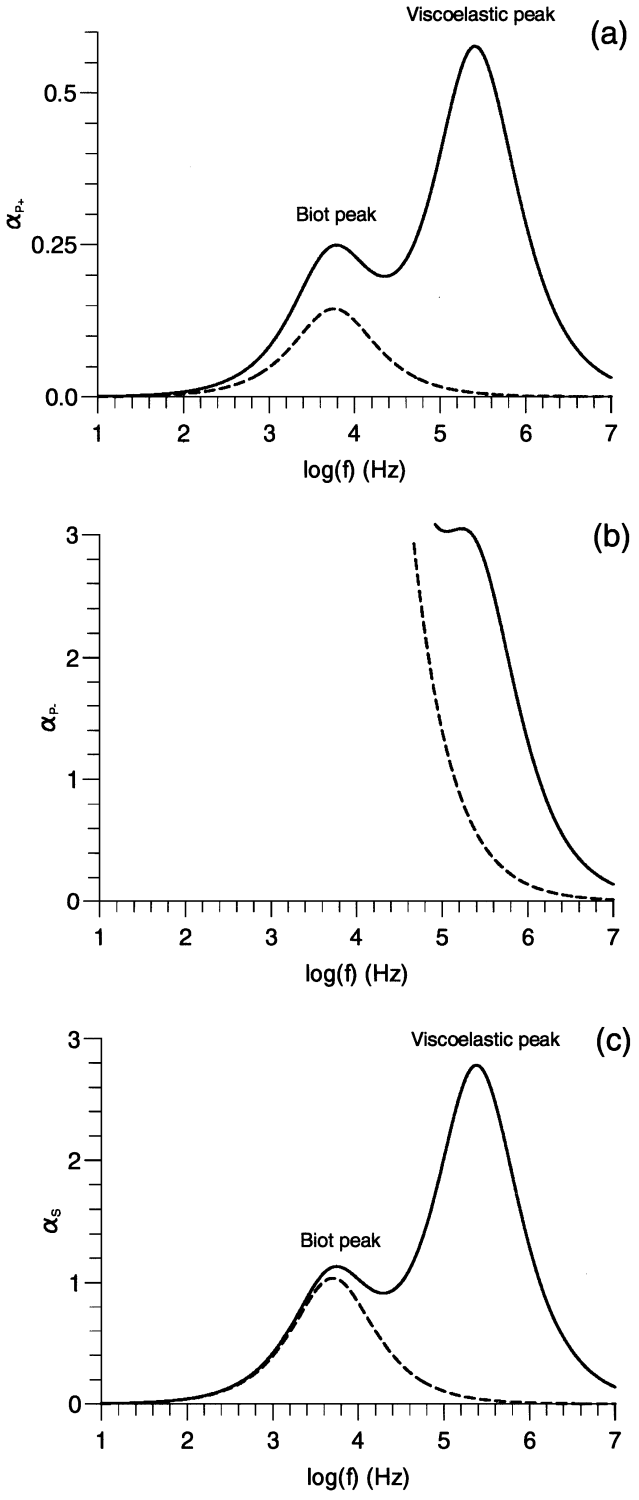

FIG. 2. Attenuation factor of the (a) fast, (b) slow, and (c) shear waves as a function of frequency. The solid lines correspond to the poroviscoelastic case; the broken lines correspond to Biot's poroelastic theory. The Biot and viscoelastic peaks can be distinguished clearly.

$s_x = s_z = \phi s_f$. Its time history is a Ricker-type wavelet and has a central frequency of 500 kHz. The poroelastic simulations are performed with an algorithm developed by Carcione and Helle (1999), which uses a fourth-order Runge-Kutta time-stepping scheme and the staggered Fourier method for computing the spatial derivatives. The stiff part of the differential equations is solved with a time-splitting technique. On the other hand, the poroviscoelastic traces are computed with a second-order Crank-Nicolson scheme (Carcione and Quiroga-Goode, 1996), the staggered Fourier method, and the splitting technique illustrated in the Appendix. Both algorithms use a time step of 0.03 μs and 3340 steps.

RESULTS AND DISCUSSION

The results of the simulation with Biot's poroelastic theory are plotted in Figure 4a. As mentioned, the discrepancies with the experimental results are from the presence of non-Biot attenuation mechanisms. The discrepancy in the F*P*-wave amplitude after the critical angle (32°C approximately) could be because the plane-wave approximation does not apply to the synthetic microseismograms, because the source is closer to the sample compared to the laboratory experiments. Figure 4b shows the poroviscoelastic microseismograms. As can be appreciated, the relative amplitudes observed are in better agreement with the experiment than those predicted by Biot's theory without viscoelastic losses. A better match can be obtained by using an inversion algorithm, but this is not within the scope of the present work.

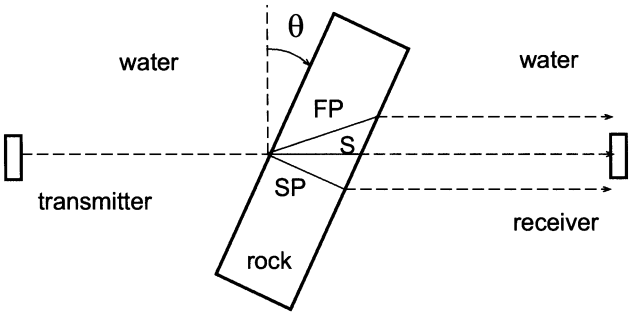

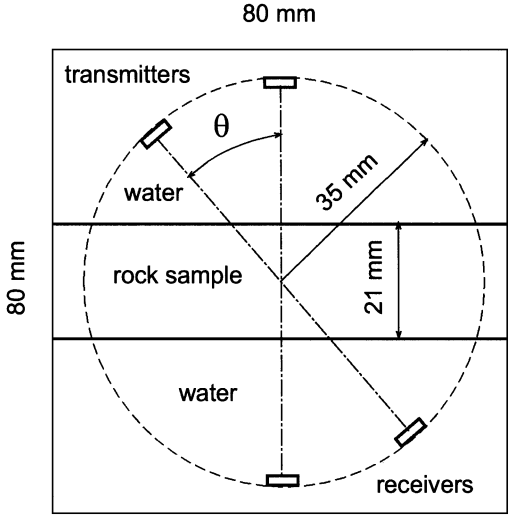

FIG. 3. (Top) Experimental setup of Kelder and Smeulders (1997). (Bottom) Model and source-receiver configuration for the simulation of the experiment *FP* denotes the fast compressional wave, *SP* denotes the slow compressional wave, and *S* denotes the shear wave.

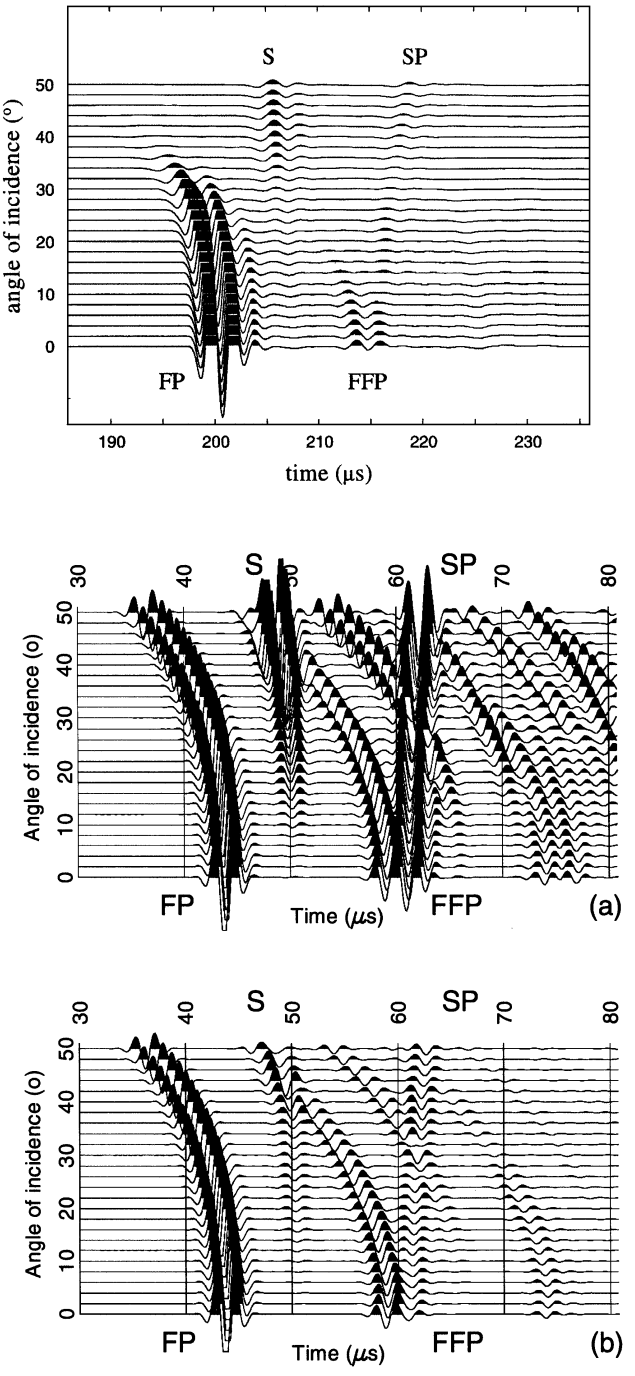

FIG. 4. Microseismogram obtained by Kelder and Smeulders (1997) for the Nivelsteiner Sandstone as a function of the angle of incidence θ (top). Numerical microseismograms obtained from (a) Biot's poroelastic theory and (b) Biot's poroviscoelastic theory. The events are the fast compressional wave (*FP*), the shear wave (*S*), the first multiple reflection of the fast compressional wave (*FFP*), and the slow wave (*SP*).

Laboratory measurements of wave velocity and attenuation factor versus frequency provide the tool for obtaining these empirical parameters and computing realistic synthetic seismograms. The observed wave attenuation in reservoir rocks can be the result of several dissipation mechanisms. Macroscopic and local fluid-flow mechanisms (Biot and squirt flow, respectively) are two such mechanisms and, in principle, can be used to fit experimental data. However, these mechanism are not enough to model the observed levels of attenuation. Moreover, the strong dependence of these models on the microstructural features makes them unreliable for attenuation prediction. A practical model, which requires calibration with controlled acoustic experiments, is the viscoelastic model parameterized by reference frequencies and quality factors associated to the stiffness moduli and the viscosity/permeability factor. It should be clear, however, that the matching between data and model results does not provide a verification about the physical cause of the attenuation. The effects can be either viscoelastic (related to the stress–strain equation) or viscodynamic (related to the kinetic energy).

CONCLUSIONS

Laboratory experiments on rock samples can provide acoustic properties (wave velocity and attenuation) under in-situ conditions (fluid composition, pore pressure, etc.) of reservoir rocks, offering a basis for physical and geological insight into lithologic interpretation of seismic data. We use Biot's theory to model ultrasonic microseismograms and obtain a calibrated seismic modeling code that can be used to compute synthetic seismograms under general conditions of material variability, since the algorithm is based on a grid method. The dry-rock moduli are obtained by fitting the shear- and compressional-wave velocities, and the tortuosity is calculated by fitting the slow-wave velocity. These three parameters—dry-rock bulk and shear moduli and tortuosity—characterize the properties of the empty skeleton and let us calculate the wet-rock properties with different pore fluids and saturation conditions. Moreover, a qualitative modeling of the relative amplitudes between the different waves provides an estimation of the attenuation at ultrasonic frequencies. The attenuation of the *S*-wave is six times higher than the attenuation of the fast *P*-wave. In fact, making viscoelastic (i.e., time dependent) the dry-rock shear moduli only, together with the coupling modulus and viscosity/permeability factor, is enough to predict the observed amplitudes.

REFERENCES

Biot, M. A., 1962, Mechanics of deformation and acoustic propagation in porous media: J. Appl. Phys., **33**, 1482–1498.

Bordakov, G. A., Ilyasov, K. K., Sekerzh-Zenkovitch, S. Y., and Mikolaevski, E. Y., 1999, Wave refraction with a porous plate in liquid—Comparison of Biot's and BISQ theories: 61st Ann. Internat. Mtg., Eur. Assoc. Expl. Geophys., Expanded Abstracts, 2-03.

Boyle, F. A., and Chotiros, H. P., 1992, Experimental detection of a slow acoustic wave in sediment at shallow grazing angles: J. Acoust. Soc. Am., **91**, 2615–2619.

Carcione, J. M., 1995, Constitutive model and wave equations for linear, viscoelastic, anisotropic media: Geophysics, **60**, 537–548.

——— 1996, Wave propagation in anisotropic, saturated porous media: Plane wave theory and numerical simulation: J. Acoust. Soc. Am., **99**, 2655–2666.

——— 1998, Viscoelastic effective rheologies for modelling wave propagation in porous media: Geophys. Prosp., **46**, 249–270.

Carcione, J. M., and Helle, H. B., 1999, Numerical solution of the poroviscoelastic wave equation on a staggered mesh: J. Comput. Phys., **154**, 520–527.

Carcione, J. M., and Quiroga-Goode, G., 1996, Some aspects of the physics and numerical modeling of Biot compressional waves: J. Comp. Acoust., **3**, 261–280.

Chin, R. C. Y., Berryman, J. G., and Hedstrom, G. W., 1985, Generalized ray expansion for pulse propagation and attenuation in fluid-saturated porous media: Wave Motion, **7**, 43–65.

Dvorkin, J., Nolen-Hoeksema, R., and Nur, A., 1994, The squirt-flow mechanism: Macroscopic description: Geophysics, **59**, 428–438.

Gurevich, B., Kelder, O., and Smeulders, D. M. J., 1999, Validation of the slow Compressional wave in porous media: Comparison of experiments and numerical simulations: Transp. in Por. Media, **36**, 149–160.

Kelder, O., and Smeulders, D. M. J., 1997, Observation of the Biot slow wave in water-saturated Nivelsteiner Sandstone: Geophysics, **62**, 1794–1796.

Johnston, D. L., Koplik, J., and Dashen, R., 1987, Theory of dynamic permeability and tortuosity in fluid-saturated porous media: J. Fluid. Mech., **176**, 379–402.

Nagy, P. B., Adler, L., and Bonner, B. P., 1990, Slow wave propagation in air-filled porous materials and natural rocks: Appl. Phys. Lett., **56**, 2504–2506.

Plona, T., 1980, Observation of a second bulk compressional wave in a porous medium at ultrasonic frequencies: Appl. Phys. Lett., **36**, 259–261.

Schmidt, H., and Tango, G., 1986, Efficient global matrix approach to the computation of synthetic seismograms: Geophys. J. Roy. Astr. Soc., **47**, 1440–1447.

Stoll, R. D., and Bryan, G. M., 1970, Wave attenuation in saturated sediments: J. Acoust. Soc. Am., **47**, 1440–1447.

Teng, Y. C., 1990, Finite elements results of the slow compressional wave in a porous medium at ultrasonic frequencies: J. Appl. Phys., **68**, 4335–4337.

APPENDIX

TIME-SPLITTING TECHNIQUE FOR BIOT'S POROVISCOELASTIC EQUATIONS

Biot's poroviscoelastic differential equations have the form $\mathbf{v}_{,t} = \mathbf{M}\mathbf{v}$, where $\mathbf{v}$ is the wavefield vector and $\mathbf{M}$ is the propagation matrix. All the eigenvalues of $\mathbf{M}$ have a negative real part. While the eigenvalues of the fast wave have a small real part, the eigenvalues of the slow wave (in the diffusive regime) have a large real part (Carcione and Quiroga-Goode, 1996). The presence of this diffusive mode makes the differential equations stiff. Then, seismic and sonic modeling are unstable when using explicit time integration methods. In both cases, the Biot peaks (i.e., the presence of the diffusive mode) make the problem stiff.

Since the presence of the slow compressional wave makes Biot's differential equations stiff, a time-splitting integration algorithm is used (Carcione and Quiroga-Goode, 1996). The evolution operator can be expressed as $\exp(\mathbf{M}_r + \mathbf{M}_s)t$, where r indicates the regular matrix and s is the stiff matrix. The product formula $\exp(\frac{1}{2}\mathbf{M}_s t)\exp(\mathbf{M}_r t)\exp(\frac{1}{2}\mathbf{M}_s t)$ is second-order accurate. The stiff part is solved analytically; the nonstiff part is solved with an A-stable second-order Crank-Nicolson scheme. This method possesses the stability properties of implicit algorithms, but the solution can be obtained explicitly.

In the following we give the solution of the stiff part in closed analytical form. Consider the x-component of the particle velocities. The stiff differential equations, including the corresponding memory variable, are

$$v_{x,t} = -\beta_{12}\left(\frac{\eta}{\kappa}\frac{\tau_\epsilon}{\tau_\sigma}q_x + e\right), \tag{A-1}$$

$$q_{x,t} = -\beta_{22}\left(\frac{\eta}{\kappa}\frac{\tau_\epsilon}{\tau_\sigma}q_x + e\right), \tag{A-2}$$

and

$$e_{,t} = -\frac{1}{\tau_\sigma}\left[\frac{\eta}{\kappa}\left(\frac{\tau_\epsilon}{\tau_\sigma} - 1\right)q_x + e\right], \tag{A-3}$$

where

$$\beta_{12} = -\frac{\rho_f}{\rho m - \rho_f^2} \quad \text{and} \quad \beta_{22} = \frac{\rho}{\rho m - \rho_f^2} \tag{A-4}$$

are components of a density matrix (Carcione, 1996; Carcione and Quiroga-Goode, 1996).

Equations (A-1)–(A-3) can be solved analytically. The intermediate field variables (indicated by an asterisk) as a function of the solution at time ndt are

$$q_x^* = m_{11}q_x^n + m_{12}e^n, \tag{A-5}$$

$$e^* = m_{21}q_x^n + m_{22}e^n, \tag{A-6}$$

and

$$v_x^* = v_x^n + \frac{\beta_{12}}{\beta_{22}}(q_x^* - q_x^n), \tag{A-7}$$

where

$$m_{11} = \frac{1}{2D}[(a_{22} - a_{11} + D)e_1 + (-a_{22} + a_{11} + D)e_2],$$

$$m_{12} = \frac{a_{12}}{D}(e_2 - e_1), \qquad m_{21} = \frac{a_{21}}{D}(e_2 - e_1),$$

$$m_{22} = \frac{1}{2D}[(a_{11} - a_{22} + D)e_1 + (-a_{11} + a_{22} + D)e_2], \tag{A-8}$$

$$e_1 = \exp\left[\frac{1}{2}(a_{11} + a_{22} - D)\,dt\right],$$

$$e_2 = \exp\left[\frac{1}{2}(a_{11} + a_{22} + D)\,dt\right] \tag{A-9}$$

$$D = \left(a_{11}^2 + 4a_{12}a_{21} - 2a_{11}a_{22} + a_{22}^2\right)^{1/2}, \tag{A-10}$$

and

$$a_{11} = -\frac{\eta}{\kappa}\frac{\tau_\epsilon}{\tau_\sigma}\beta_{22}, \qquad a_{12} = -\beta_{22},$$

$$a_{21} = -\frac{\eta}{\kappa}\frac{1}{\tau_\sigma}\left(\frac{\tau_\epsilon}{\tau_\sigma} - 1\right), \qquad a_{22} = -\frac{1}{\tau_\sigma}. \tag{A-11}$$

The starred field variables are the input for a Crank-Nicolson scheme that solves the poroviscoelastic equations with $\eta = 0$. The result is the solution at time $(n+1)\,dt$. A similar solution applies to the z-component of the particle velocities.

The spatial derivatives are calculated with the staggered Fourier method by using the fast Fourier transform (FFT) (Carcione and Helle, 1999). This approximation is infinitely accurate for band-limited periodic functions with cutoff spatial wavenumbers which are smaller than the cutoff wavenumbers of the mesh.